

POLARIMETRIC OBSERVATIONS OF SNOW GROWTH IN STRATIFORM CLOUDS

Jonathan M. Vogel *, Frédéric Fabry, and Isztar Zawadzki
 Department of Atmospheric and Oceanic Sciences, McGill University, Montreal, QC, Canada

1. Introduction

Extensive research has been done on the many polarimetric signatures detected during severe convective events; however, there continues to be a lack of understanding of ice crystal habits, especially in stratiform clouds. With the completion of upgrading the WSR-88D radars to dual-polarization, on an operational sense, understanding these signatures has become even more paramount. Recently, studies have observed an enhancement of K_{dp} and Z_{dr} above the bright band near the -15°C region in stratiform clouds (Kennedy and Rutledge, 2011; Andrić et al., 2013; Bechini et al., 2013; Schneebeli et al., 2013). The difference between supersaturation over ice versus water is a maximum in this region. Also, at these temperatures, growth along the lateral axis is favored (Bailey and Hallett, 2009). Preferential growth of ice crystals along the same axis should produce increases in Z_{dr} first, due to shape, followed by K_{dp} , due to mass (Kennedy and Rutledge, 2011; Schneebeli et al., 2013). Once the particles become large enough or after growth by diffusion becomes less significant, processes such as aggregation and/or riming should change the shape and density of the ice crystals leading to a change in the signatures of the variables. Previously, aggregation was thought as the dominant growth mechanism at temperatures warmer than -15°C , but with the addition of a vertically pointing radar, observations of increases in fall speed may indicate when riming plays a more important role in crystal growth.

2. Radar Data

The J.S. Marshall Radar Observatory in Dorval, QC features several instruments, including an S-band polarimetric radar and an X-band vertically pointing Doppler radar (VertiX). The S-band radar scans of the atmosphere at 24 elevations between 0.5° and 34.4° every 5 minutes providing polarimetric variables, including reflectivity (Z), differential reflectivity (Z_{dr}), specific differential phase (K_{dp}), and correlation coefficient (ρ_{hv}). Every 2 seconds the

VertiX retrieves reflectivity (Z_v) and Doppler velocity (V_i) observations.

For this study, stratiform cases were chosen from a 10 km by 58° box 20 km northwest of the radar site from September 2011 to October 2012. Corresponding VertiX data from the radar observatory site was matched to the event occurring in the box to the northwest. 40 cases were used for a total of 28.2 hours of data. For data quality purposes, points within a 5 by 5 grid of an S-band data point were checked and those with Z less than 0 dBz , ρ_{hv} less than 0.80 , or a target ID of ground or biological scatterer were removed.

This paper features a unique way of plotting polarimetric radar data as a function of both height above the bright band and reflectivity (Figure 1). At a given time, each polarimetric variable observation has a corresponding height and reflectivity value. The data is binned every 2 dBz and 0.2 km , and then averaged over a certain time period to produce images similar to Figure 1. Presenting the data in this manner allows for two distinct advantages when observing the growth of hydrometeors. First, since temperature varies as a function of height, changes in polarimetric signatures may be observed at critical temperature thresholds within the atmosphere. Second, because reflectivity is largely a function of mean size, different changes in polarimetric signatures may be observed at different mean hydrometeor sizes. Together, plotting polarimetric variables in this method allows for observation of microphysical processes both as a function of temperature and particle size.

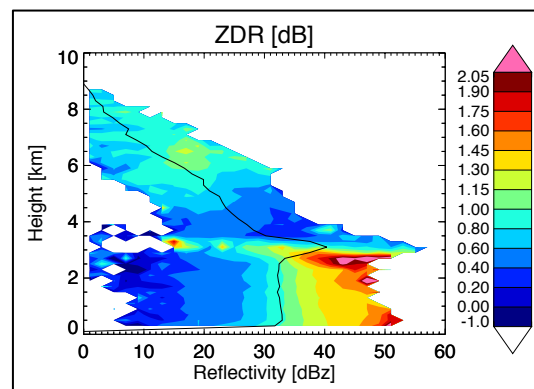


Figure 1. Example Z_{dr} plot from 19:39z to 20:09z on October 14, 2011.

* Corresponding author address: Jonathan M. Vogel, Atmospheric and Oceanic Sciences, Burnside Hall 805 Sherbrooke Street West, Montreal, QC, Canada, H3A 0B9

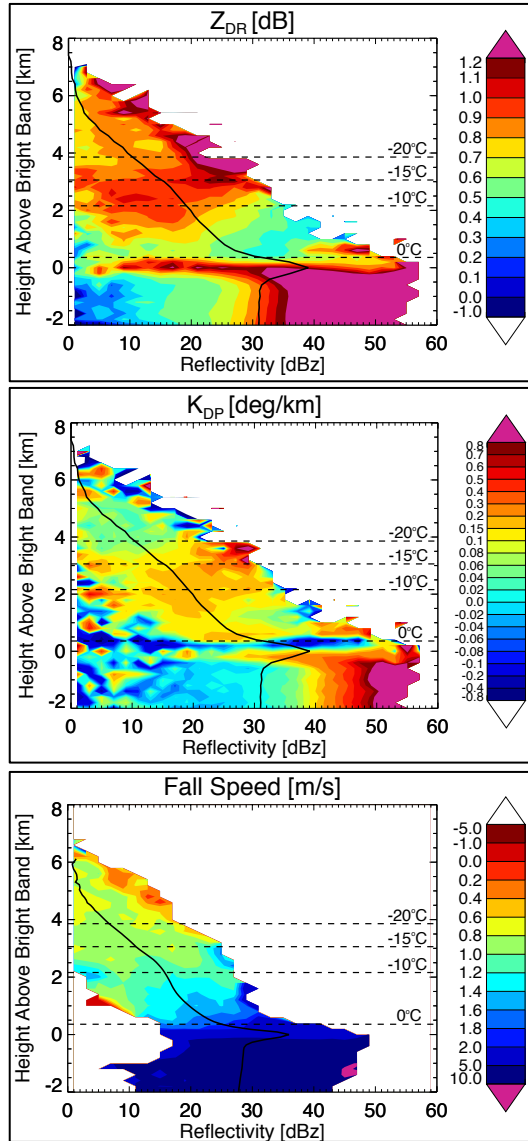


Figure 2. (Top) Z_{dr} , (Middle) K_{dp} , and (Bottom) V_f signatures, averaged over all high reflectivity cases.

3. Results

During the period of study, three different families of data became evident. The cases were separated into these families based on polarimetric signatures above the bright band as well as Z , Z_{dr} , and V_f observations in rain. The two primary families consisted of high and low reflectivity cases. The threshold for each of these cases was a Z of 30 dBz, a Z_{dr} of 0.7 dB, and a V_f of 6.5 m s^{-1} . High reflectivity cases were those with surface values above the thresholds while low reflectivity cases were those with surface values below the thresholds. The third grouping, hybrid cases, consisted of cases during which the surface conditions fit that of high reflectivity while the polarimetric signatures above

the bright band were more similar to that of the low reflectivity family.

3.1 High Reflectivity

The high reflectivity family consists of 16 cases for about 10.3 hours of data. For this family, in the region near -15°C Z_{dr} shows a localized maxima (Figure 2). From previous studies, favored growth along the lateral axis is expected in this temperature range, which could lead to an increase in Z_{dr} (Korolev et al., 2000; Bailey and Hallett, 2009; Schneebeli et al., 2013). The largest crystals appear to activate sooner, closer to -20°C , while the smallest crystals activate later, closer to -10°C . K_{dp} shows a similar peak, but at slightly lower altitudes since K_{dp} is more affected by the ice crystal mass (Figure 2). Z also shows faster growth in this region as ice crystals grow fastest since the difference in supersaturation over ice and water is greatest in this region.

At warmer temperatures, growth by diffusion becomes less significant and ice crystals grow by another mechanism. One possibility is aggregation, as the particles would become more spherical and less dense reducing both Z_{dr} and K_{dp} signatures. Another possibility is riming, as it would result in an increase in axis ratios thereby decreasing both Z_{dr} and K_{dp} . In Figure 2, fall speed observations show speeds increase rapidly to faster than 1.5 m s^{-1} above the bright band, which indicates riming is likely significant (Mossiman et al., 1993; Zawadzki et al., 2001). It is unlikely that only one process is taking place, but together, they should produce the observed Z_{dr} and K_{dp} profiles.

As the ice crystals fall into the melting layer, the expected signatures of Z_{dr} and Z enhancement, fall speed increase, and the pair of positive and negative K_{dp} values are seen (Brandes and Ikeda, 2004). However, an additional region of slightly enhanced K_{dp} values is also seen above and slightly reduced K_{dp} values are seen below the bright band. We speculate this is due to a slight difference in the beam widths of the horizontal and vertical pulses.

Below the bright band, Z is greater than 30 dBz, Z_{dr} is greater than 0.7 dB, and V_f is greater than 6.5 m s^{-1} , which implies larger raindrops are present near the surface. To achieve larger raindrops, significant growth must have occurred above the bright band.

3.2 Low Reflectivity

The low reflectivity family consists of 18 cases for about 13 hours of data. Like in the high reflectivity family, ice crystals should experience preferential lateral axis growth in the region near -15°C . Growth along the lateral axis can be supported by a peak in Z_{dr} near -15°C along with

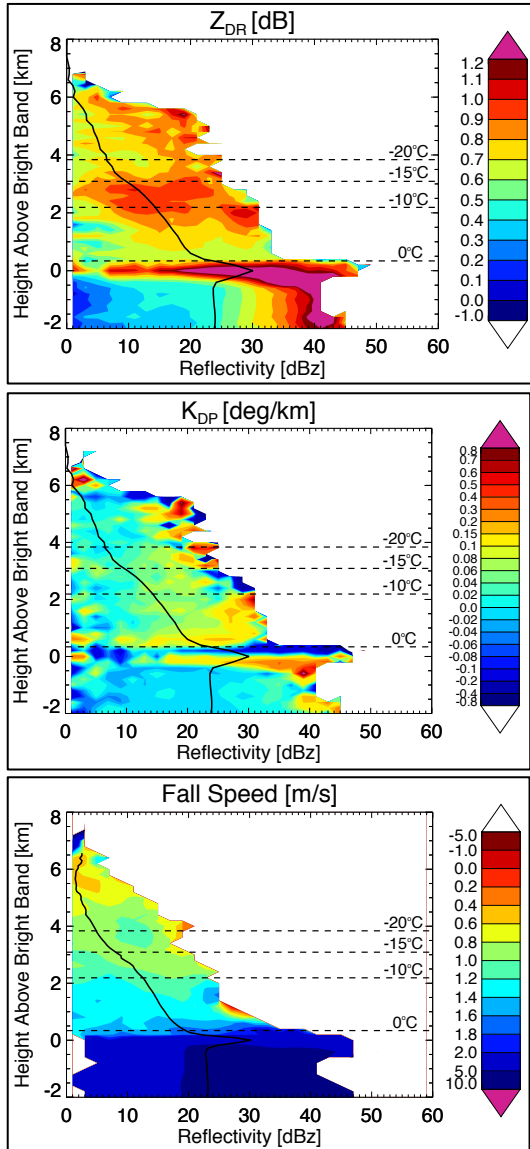


Figure 3. (Top) Z_{dr} , (Middle) K_{dp} , and (Bottom) V_f signatures, averaged over all low reflectivity cases.

a large increase Z in this region (Figure 3). However, in this family, the Z_{dr} peak occurs uniformly at all reflectivities while K_{dp} only shows a slight increase (Figure 3). Since K_{dp} is related to ice water content (Bringi and Chandrasekar, 2001), the lack of K_{dp} peak implies a smaller amount of ice is present in these cases.

At warmer temperatures, Z_{dr} decreases with increasing Z suggesting some aggregation is taking place. K_{dp} remains relatively constant at all reflectivities and V_f stays below the riming threshold (Figure 3). The K_{dp} and V_f signatures suggest that K_{dp} could be affected more by riming than by aggregation than previously thought.

Below the bright band, Z is less than 30 dBz, Z_{dr} is less than 0.7 dB, and V_f is less than 6.5 m

s^{-1} , which imply smaller raindrops are present near the surface. The presence of smaller raindrops implies that there was less growth above the bright band in this family.

3.3 Hybrid Cases

The hybrid cases consist of 6 cases for about 4.9 hours of data. This family was classified as hybrid since near the surface they appeared similar to the high reflectivity family, but above the bright band they had a mixture of polarimetric signatures. Near the -15°C region, Z_{dr} peaked likely due to preferential lateral axis growth coincident with an increase in Z (Figure 4). For this family, higher reflectivities peaked in Z_{dr} sooner, similar to the high reflectivity family.

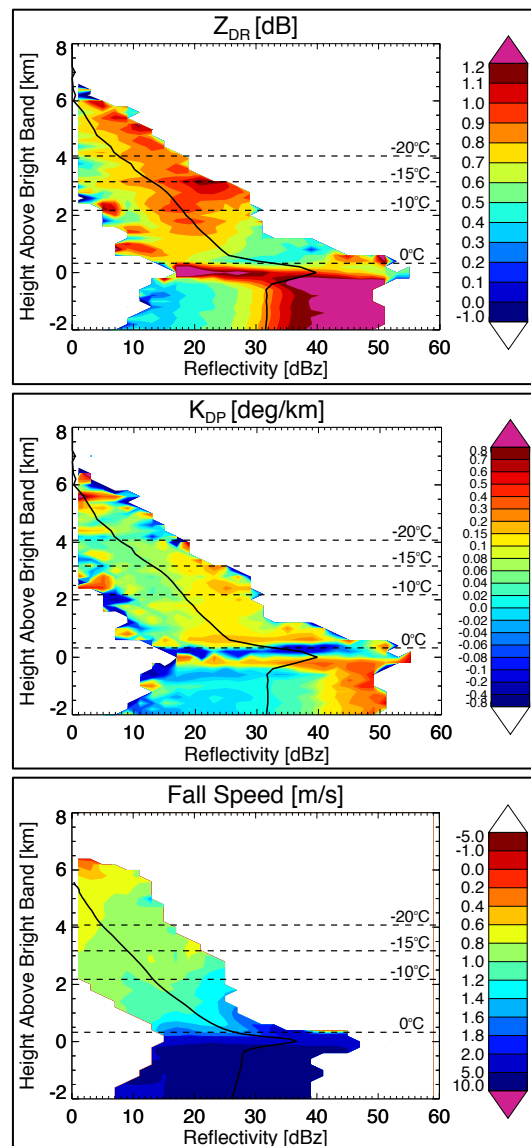


Figure 4. (Top) Z_{dr} , (Middle) K_{dp} , and (Bottom) V_f signatures, averaged over all hybrid cases.

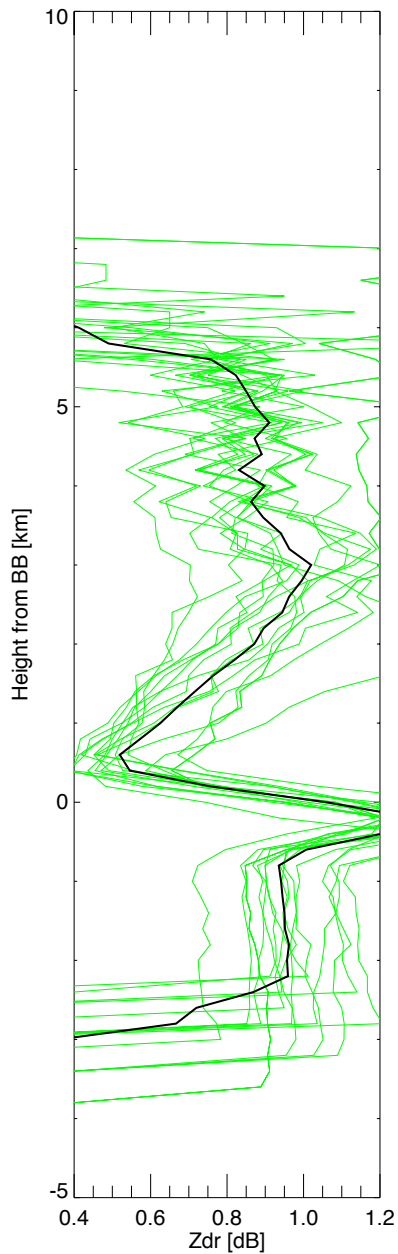


Figure 5. Mean of the Z_{dr} profile for each height level for the high reflectivity cases illustrated in Figure 2.

However, K_{dp} showed only a slight peak, which is similar to the low reflectivity family (Figure 4).

At warmer temperatures, as aggregation is expected to dominate, Z_{dr} decreases and declines the fastest at higher reflectivities. Generally K_{dp} remains constant with height, but at the highest reflectivities, K_{dp} decreases slightly while V_f shows a rapid increase to greater than 1.5 m s^{-1} indicating that some riming is likely (Figure 4).

Below the bright band, Z is greater than 30 dBz, Z_{dr} is greater than 0.7 dB, and V_f is greater

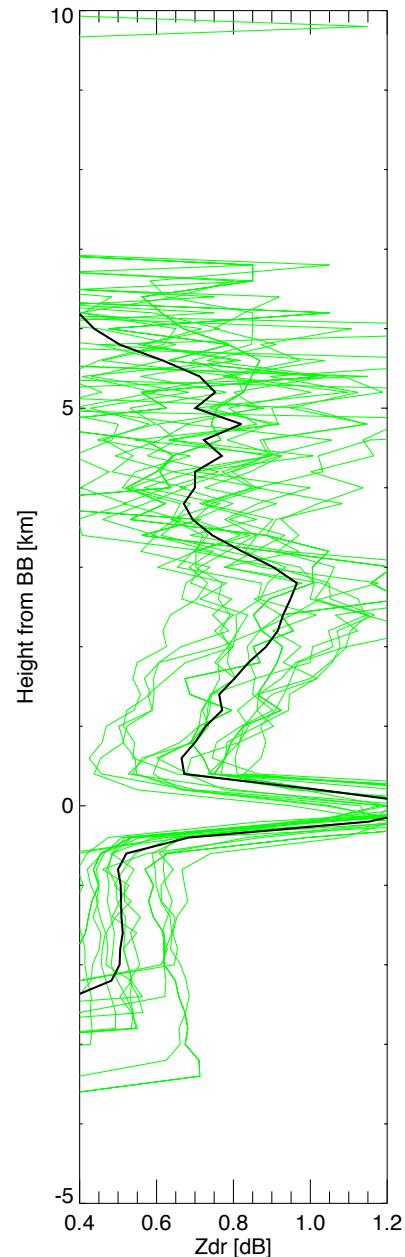


Figure 6. Same as Figure 5, but for the low reflectivity cases.

than 6.5 m s^{-1} , which implies larger raindrops are present near the surface. Above the bright band, most of the polarimetric signatures indicated the likelihood of smaller drops at the surface; however, the presence of riming at high reflectivities just above the bright band could be the cause of larger drops below.

4. Discussion

In all three families, Z_{dr} shows a peak in the region where preferential growth along the lateral

axis is expected. Once aggregation becomes significant, a decrease in Z_{dr} can be seen in all three families. Previous studies have shown this transition from preferential growth to aggregation as more of a gradual process (Kennedy and Rutledge, 2011; Andrić et al., 2013; Bechini et al., 2013; Schneebeli et al., 2013); however, in Figures 5 and 6, the Z_{dr} shows an abrupt change in slope, which cannot be fully explained at this time.

From temperatures around the -15°C level and below, K_{dp} shows at least a slight increase in all three cases. This could be associated with an increase in ice crystal mass due to the preferential growth. However, unlike Z_{dr} , K_{dp} does not show similar trends in all three families at warmer temperatures. Based on fall speed observations, in regions in which riming may be present, K_{dp} also shows a decrease. This suggests that aggregation may have less of an impact on K_{dp} than riming.

On average, to achieve larger raindrops at the surface, V_f observations from the VertiX suggest some riming must be present to complement growth by aggregation above the bright band. When V_f does not reach the 1.5 m s^{-1} threshold, generally smaller raindrops can be expected at the surface. The V_f observations suggest aggregation alone is not efficient enough to produce larger raindrops.

5. References

- Andrić, J., M. R. Kumjian, D. S. Zrnić, J. M. Straka, and V. M. Melnikov, 2013: Polarimetric signatures above the melting layer in winter storms: an observational and modeling study, *J. Appl. Meteor. Climatol.*, 52, 682-700.
- Bailey, M. P., and J. Hallett, 2009: A comprehensive habit diagram for atmospheric ice crystals: confirmation from the laboratory, AIRS II, and other field studies. *J. Atmos. Sci.*, 66, 2888-2899.
- Bechini, R., L. Baldini, and V. Chandrasekar, 2013: Polarimetric radar observations in the ice region of precipitating clouds at C-band and X-band radar frequencies, *J. Appl. Meteor. Climatol.*, 52, 1147-1169.
- Brandes, E. A., and K. Ikeda, 2004: Freezing-level estimation with polarimetric radar, *J. Appl. Meteor.*, 43, 1541-1553.
- Bringi, V. N., and V. Chandrasekar, 2001: *Polarimetric Doppler Weather Radar: Principles and Applications*. Cambridge University Press. 479-480 pp.
- Kennedy, P. C. and S. A. Rutledge, 2011: S-band dual-polarization radar observations of winter storms, *J. Appl. Meteor. Climatol.*, 50, 844-858.
- Korolev, A., G. A. Isaac, and J. Hallett, 2000: Ice particle habits in stratiform clouds. *Quart. J. Roy. Meteor. Soc.*, 126, 2873-2902.
- Mosimann, L., M. Steiner, and W. Henrich, 1993: Prediction of snow crystal shape and riming by vertical Doppler radar, *Atmos. Res.*, 29, 85-98.
- Schneebeli, M., N. Dawes, M. Lehning, and A. Berne, 2013: High-resolution vertical profiles of x-band polarimetric radar observations during snowfall in the Swiss Alps, *J. Appl. Meteor. Climatol.*, 52, 378-394.
- Zawadzki, I., F. Fabry, and W. Szyrmer, 2001: Observations of supercooled water and secondary ice generation by a vertically pointing X-band Doppler radar, *Atmos. Res.*, 59-60, 343-359.

